End-to-End Stacking and Liquid Crystal Condensation of 6–to 20–Base Pair DNA Duplexes

Michi Nakata,[1]*† Giuliano Zanchetta,[2]* Brandon D. Chapman,[3] Christopher D. Jones,[1] Julie O. Cross,[4] Ronald Pindak,[3] Tommaso Bellini,[2]‡ Noel A. Clark[1]‡

Short complementary B-form DNA oligomers, 6 to 20 base pairs in length, are found to exhibit nematic and columnar liquid crystal phases, even though such duplexes lack the shape anisotropy required for liquid crystal ordering. Structural study shows that these phases are produced by the end-to-end adhesion and consequent stacking of the duplex oligomers into polydisperse anisotropic rod-shaped aggregates, which can order into liquid crystals. Upon cooling mixed solutions of short DNA oligomers, in which only a small fraction of the DNA present is complementary, the duplex-forming oligomers phase-separate into liquid crystal droplets, leaving the unpaired single strands in isotropic solution. In a chemical environment where oligomer ligation is possible, such ordering and condensation would provide an autocatalytic link whereby complementarity promotes the extended polymerization of complementary oligomers.

The ability of duplex DNA to form liquid crystal (LC) phases when hydrated has been known since the late 1940s and played a crucial role in deciphering its structure, enabling alignment of the DNA chains and measurement of the x-ray structure factor of a single chain uncomplicated by interchain correlations (1–3). Since that time, the LC phases of solutions of duplex B-form DNA (B-DNA) have been extensively characterized by optical (4–9), x-ray (10), and magnetic resonance (11, 12) methods for chain lengths N, ranging from mega–base pair (bp) semiflexible polymers down to approximately 100 bp rigid rodlike segments, comparable in size to the B-DNA bend persistence length, $\Lambda_p \sim 50$ nm (13). These studies of long DNA (lDNA) have revealed an isotropic phase (I); chiral nematic (N), uniaxial columnar (C_U), and higher-ordered columnar (C_2) liquid crystal phases; and crystal (X) phases, with increasing DNA concentration.

The appearance of such LC phases has been accounted for theoretically by modeling B-DNA as a repulsive rigid or semiflexible rod-shaped solute. The basic model is Onsager's treatment of monodisperse repulsive hard rods (length L, diameter D) (14), which, if they are sufficiently anisotropic in shape, nematic order for volume fraction $\varphi > \varphi_{I\text{-}N} = 4D/L \approx 24/N$ ($D \sim 2$ nm, $L \sim N/3$ nm for B-DNA). The complete computer-simulated phase diagram for hard rods by Bolhuis and Frenkel (15) quantitatively confirms this prediction for $L/D > 4.7$ ($N > 28$ bp) and also shows that for $L/D < 4.7$ there should be no LC phases at any φ. We were therefore surprised to find nematic LC ordering in short B-DNA duplexes (sDNA) of length 6 bp $< N <$ 20 bp, with the nematic phase appearing for N values an order of magnitude smaller than those predicted from φ_{IN}, precluding ordering by the Onsager-Bolhuis-Frenkel (OBF) criterion. A similar conclusion was reached by Alam and Drobny in attempting to account for a magnetically reorientable, orientationally ordered phase in nuclear magnetic resonance studies of a B-DNA dodecamer (12). Additionally, we have observed columnar LC ordering for these oligomers, which is also notable, because in the hard-rod models (15), the only translationally ordered LC phase appearing is the lamellar smectic A (SmA). We show that the observation of the nematic and columnar LC phases provides clear evidence for end-to-end stacking of the sDNA into rod-shaped aggregates. The sensitivity of the aggregation to complementarity leads directly to a means of phase separation of complementary sDNA duplexes from a solution of complementary and noncomplementary oligomers.

We studied the series of self-complementary sDNA duplex-forming "palindromic" oligomers shown in Fig. 1, along with a variety of noncomplementary and partially complementary oligomers (16). sDNA solutions in gaps of thickness t between glass plates (4 μm $< t <$ 8 μm) were observed by (i) depolarized transmission light microscopy (DTLM) to probe optical textures, (ii)

Fig. 1. Optical textures of the LC phases of a series of solutions of sDNA of increasing length obtained by depolarized light microscopy. Samples thickness is in the range 4 μm $< t <$ 8 μm, between glass plates. Isotropic (I) regions are black. The chiral nematic phase (N) appears as fluid birefringent domains when its helix pitch is a few microns or longer, or, when the pitch is shorter than ~400 nm, as a Grandjean texture with "oily streaks" exhibiting visible light selective reflection from the macroscopic optic axis helix (8 bp, 10 bp). The columnar C_U phase is identified by its smooth developable domains, a consequence of the uniaxial symmetry and splay expulsion of the columnar ordering. At yet higher DNA concentration, the C_2 phase exhibits dendritic growth forms, indicative of lower symmetry and more solidlike ordering. The width of each image is 120 μm.
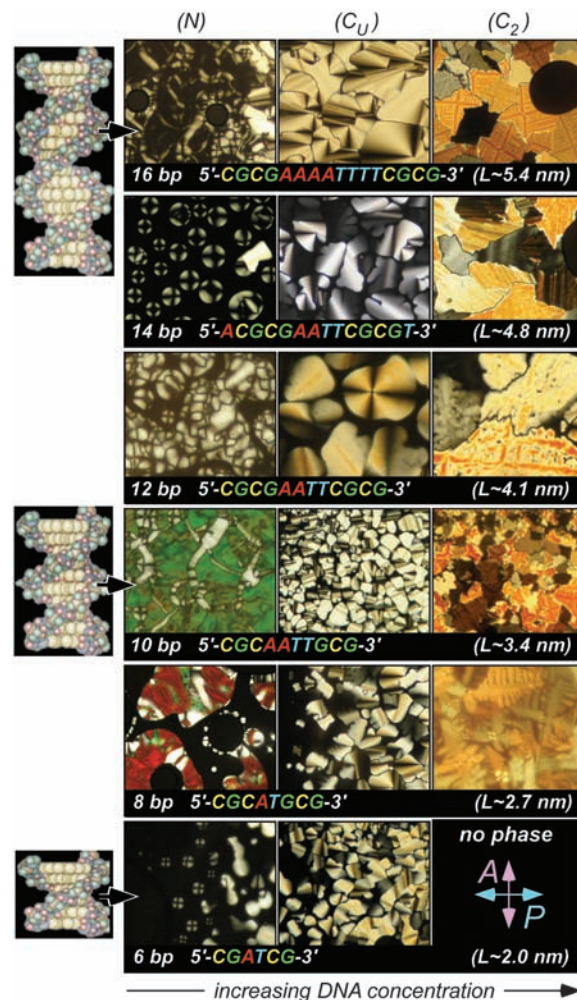
[1]Department of Physics and Liquid Crystal Materials Research Center, University of Colorado, Boulder, CO 80309–0390, USA. [2]Dipartimento di Chimica, Biochimica e Biotecnologie per la Medicina, Università di Milano, Milano, Italy. [3]National Synchrotron Light Source, Brookhaven National Laboratory, Upton, NY 11973, USA. [4]Advanced Photon Source, Argonne National Laboratory, Argonne, IL 60439, USA.

*These authors contributed equally to this work.
†Deceased.
‡To whom correspondence should be addressed. E-mail: tommaso.bellini@unimi.it (T.B.); noel.clark@colorado.edu (N.A.C.)

optical reflection interferometry (ORI) to measure refractive indices and thus DNA concentration c (mg solute/ml solution), and (iii) synchrotron microbeam x-ray diffraction (XRD) to probe local molecular organization. Despite the challenges presented by the extremely small sDNA sample quantities available, these techniques provided unambiguous evidence for the N and C_U liquid crystal phases in the sDNA solutions. At higher concentration, more ordered C_2 and X-like phases, which are yet to be characterized, were also found. Figure 1 shows DTLM images of the typical textures. Observation of the local optical texture and ORI measurement of the local concentration of the palindromic oligomers enabled construction of the N-c phase diagrams of Fig. 2 and figs. S1 and S2 (16). Figure 2 combines the phase boundaries measured for sDNA with those obtained from the literature for lDNA (fig. S1A), along with the predictions from the Onsager and other models of interacting semiflexible rod-shaped particle and aggregate solutes (fig. S1B). The sDNA solutions

exhibited thermotropic mesomorphism, melting at sufficiently high temperature, T, to the optically isotropic liquid (I) phase. This is shown in fig. S2, where we plot T_{LC}, the highest T at which the N and C_U phases are found. T_{LC} grows with N and, for each oligomer, is higher for the C_U phase (16).

Figure 2 shows that LC phases are found in the sub-Onsager region of the phase diagram of sDNA where they are not expected on the basis of duplex shape. When analyzed in the context of the extensive body of theory of the phase behavior of interacting rods, semiflexible polymers, and self-assembled linear aggregates, this phase diagram presents clear evidence that the origin of the LC phases in sDNA is the equilibrium end-to-end physical aggregation (living polymerization) of short duplexes into extended duplex units that are long and rigid enough to order. The key observations are as follows: (i) The sDNA LC phases have all the basic features of the LC ordering of lDNA: N phase, a state of negative optical anisotropy, miscible with the lDNA nematic and exhibit-

ing a chiral helical precession of the director producing Bragg reflection (Fig. 1 and fig. S3); C_U phase, at higher concentration, an optically uniaxial phase exhibiting an XRD structure of hexagonally packed columns lacking positional correlation along their axes (fig. S4). (ii) Nematic and columnar LC ordering can be induced in weakly anisotropic solutes by equilibrium end-to-end self-assembly, that is, living polymerization of the oligomers into linear chains of particles (17–19). Computer simulations (18–20) show that for sufficiently rigid aggregate chains, the I-N transition occurs according to the OBF prediction if the average aggregate length $\langle L \rangle$ is used in the OBF model [green dots and construction in Fig. 2A (18)]. Rigidity is a key requirement, because even infinitely long flexible hard rods (21) must have a sufficiently long persistence length for a nematic phase to appear ($\Lambda_p > \sim 10 \ D$). (iii) End-to-end adhesion suppresses the lamellar SmA phase predicted for monodisperse hard rods by favoring end-to-end rather than side-by-side positional correlations and by introducing unavoidable length polydispersity into the ordering units, both effects reducing the entropic free energy gain of lamellar ordering. (iv) Estimates of the stacking energy between duplexes are consistent with end-to-end attraction resulting from the hydrophobicity of the faces of their terminal base pairs (16, 22). This sort of assembly is familiar in crystalline sDNA (23) and in sDNA/protein complexes (24, 25), as well as in chromonic LCs (26), and has been extensively studied for particular DNA bases; for example, guanosine forms H-bonded tetramers, which aggregate into stacks (27). We show here that such aggregation, sketched in Fig. 3A, can have a substantial effect on the organization and phase behavior of B-form DNA. Although the duplexes individually are not anisotropic enough in steric shape to produce LC phases, the hydrophobic ends cause the formation of much more anisotropic assemblies that can orientationally and positionally order.

Figure 2A shows that the lDNA I-N phase boundary measured for 100 bp $< N <$ 8000 bp (8, 11) is in reasonable agreement with the simple Onsager rigid-rod limit (OBF line, fig. S1) if the effective double-helix diameter is taken to be D_{eff} = 4.0 nm to account for the electrostatic repulsion between chains at low c (8). The choice D_{eff} = 4.0 nm also puts the lDNA experimental N-C_U phase boundary (7, 10) at φ_{N-CU} = 0.55, in agreement with models of long polydisperse rods [Taylor, Bates, Bohle (TBB) line] (fig. S1) (17, 28, 29). However, as the oligomer length is decreased, the C_U phase and the nematic phase persist for duplexes as short as N = 6, although the c required to obtain these phases increases with decreasing N. For N = 6, the N-C_U transition is found at c = 1,200 mg/ml, about two-thirds that of neat duplex DNA $c_{DNA} = \rho_{DNA}$ = 1,800 mg/ml (30). Thus, the LC phases of the oligomers of
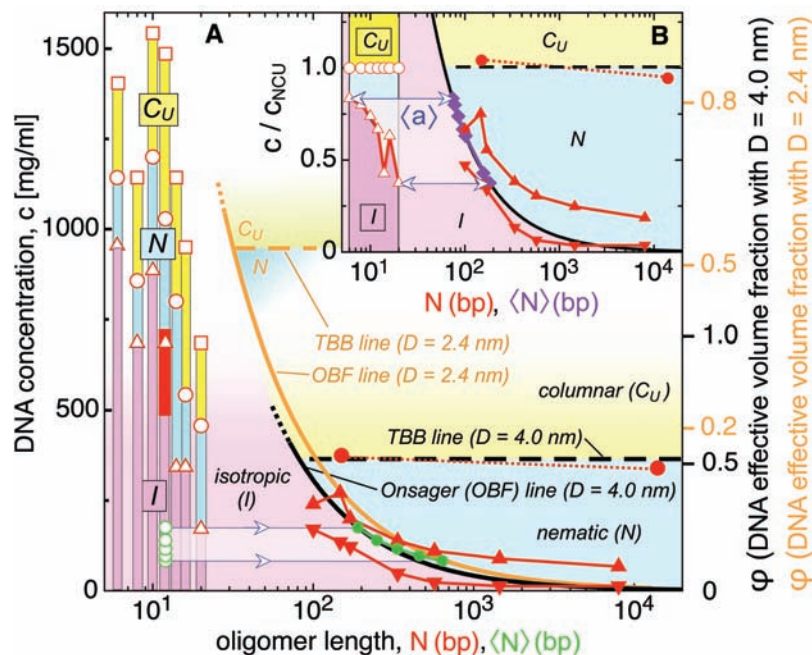

Fig. 2. Experimental c (DNA concentration, mg solute/ml solution) - N (oligomer length) phase behavior for short and long DNA (sDNA and lDNA, respectively) (fig. S1A), along with the theoretical behavior from several models of interacting rodlike particles (fig. S1B). (**A**) The solid red triangles and solid red curve bound the measured I-N phase coexistence for lDNA (N > 100) (8, 11). The solid red circles and red dotted line give the measured N-C_U phase boundary of lDNA (7, 10). For N < 20, phase transitions from our data are marked by red open symbols (I-N, triangles; N-C_U, circles; C_U-C_2, squares), and the range of each phase is indicated by colored columns (I, magenta; N, cyan; C_U, yellow), at T = 20°C for N < 20 and T = 10°C for N = 6. The range of the N = 12 LC phase of (12) is given by the solid red rectangle. Theoretical phase boundaries for these transitions from model systems are shown for two choices of the volume fraction φ axis, one with the DNA effective electrostatic diameter D = 4.0 nm (heavy black lines/labels), applicable at low c, and the other with the DNA chemical diameter D = 2.4 nm (21) (heavy orange lines/labels), applicable at high c, i.e., small N. The D = 4.0 nm phase diagram [black OBF I-N line and dashed black TBB N-C_U line (fig S1) (15, 17–19)] accounts well for the lDNA I-N and N-C_U data. The open and closed green dots represent, respectively, the spherical particles of the Lu and Kindt simulations [$L = D$ = 4.0 nm (18)], and their effective aggregate lengths $\langle N \rangle$ at the I-N transition. (**B**) The c-N phase diagram of (A), but with c scaled with respect to c_{N-CU}, enabling an estimate of the length $\langle N \rangle$ (purple diamonds), and aggregation number $\langle a \rangle$ (blue arrows) in the sDNA aggregates.

smallest N may be better viewed as being like thermotropic LC phases, their interaxial distance approaching the chemical diameter (*10, 31*) where steric repulsion dominates the interchain interactions. Hence, the increasing φ_{N-CU} observed with decreasing N indicates that the effective chain diameter decreases, evolving from $D \sim 4.0$ nm to $D \sim 2.4$ nm. This change shifts the model phase boundaries in Fig. 2A to higher concentration (black φ scale → orange φ scale) to account for the increased concentration necessary for LC phase formation. The open green dots represent the spherical particles of Lu and Kindt (*18*) ($L = D = 4.0$ nm), and the construction with the closed green dots gives $\langle N \rangle$, the effective lengths in base pairs of the aggregates at which the N phase appears in their simulations. These lengths match the OBF line well, indicating that the model aggregates behave effectively as hard rods, justifying the similar construction in Fig. 2B.

This effective diameter variation is scaled out in Fig. 2B, where the c axis is normalized by c_{N-CU}, assuming the sDNA concentration at the N-C_U transition (c_{N-CU}) to correspond, for each oligomer, to an effective volume fraction $\varphi_{N-C} \sim 0.55$ (*17–19*). That is, we select the appropriate D for a given oligomer by requiring the N-C_U transition to occur at $\varphi \sim 0.55$. Figure 2B then enables analysis of the sDNA end-to-end stacking, because once the effective volume

fraction is held by the strict requirement placed by the N-C_U transition, the amount of linear aggregation can be evaluated by horizontally projecting the I-N data points onto the black OBF line (blue arrows) for linear aggregation. The blue arrow construction thus gives an estimate of $\langle N \rangle$ (purple diamonds), and $\langle a \rangle$ (blue arrows), respectively the mean number of base pairs and the mean number of duplex oligomers in an aggregate necessary to generate an Onsager nematic. For $N = 6, 8, 10, 12, 14, 16,$ and 20 bp, oligomers $\langle a \rangle$ and $\langle N \rangle$, obtained from Fig. 2B, are, respectively, $\langle a \rangle = 12, 9, 9, 8, 11, 6,$ and 9 bp and $\langle N \rangle = 75, 80, 87, 97, 100, 160,$ and 180 bp. The decreasing aggregate length needed for nematic order for shorter oligomers is a result of their higher concentration. The aggregation number does not depend strongly on N. Figure 2B also shows that the nematic range decreases, and thus that the flexibility of the aggregates increases with decreasing N (*20, 21*).

From these lengths and the sDNA concentrations, it is possible to estimate the end-to-end stacking energy ΔE_S between the duplexes, where ΔE_S represents the difference between the energy of a stacked pair of duplexes relative to their mean status, which is strong repulsion, as shown by the substantial osmotic pressures in the N and C_U phases in the experiments of Podgornik *et al.* (*10*). Estimates for ΔE_S from

expressions proposed to describe the living polymer mean aggregate length (*18, 22, 32*) lead to 4 $k_B T < \Delta E_S < 8$ $k_B T$ per contact [equations S2 to S5 (*16*)], in addition to $T\Delta S_\Theta$, ~ 6 $k_B T$, the minimal orientational free energy cost of establishing common duplex axes in an aggregate (equation S1). None of the estimates show significant N dependence.

The requirement of developing sufficient shape anisotropy and rigidity in the aggregate units puts considerable constraints on the sDNA structure in order for LC phases to appear. Thus, sequence substitutions reducing the ability of the sDNA duplexes to form linear rigid aggregates will reduce the stability of the LC phases. For example, the addition of unpaired bases at the sDNA duplex ends, eliminates LC ordering by weakening end-to-end adhesion (*16*). This interplay of sequence and LC ordering leads to a remarkable means of condensation of complementary sDNA duplexes from mixed solutions of complementary and noncomplementary oligomers. This process is sketched in and demonstrated in Fig. 3C for a mixture of the mutually complementary, but not self-complementary, CCTCAAAACTCC (Z) + GGAGTTTTGAGG (Y) 12-nucleotide oligomers. In such a solution, at $T < T_m$, the DNA denaturation temperature, the complementary pairs form rigid duplexes that have a tendency to aggregate end-to-end, whereas the noncomplementary oligomers remain as flexible single strands. The LC ordering shows up via a first-order phase transition in which the appearance of the LC transition is accompanied by nearly complete phase separation of the duplexes into the LC domains, with the highly flexible (*33*) single strands left unbound in the isotropic phase. This phase separation can be understood on the basis of either the depletion interaction (*34*) or the immiscibility of rigid and flexible polymer solutes (*35, 16*). If there is a large excess of noncomplementary oligomers, in this case $c_Y/c_Z = 10$, the LC phase appears as isolated drops (Fig. 3D). The dependence of the phase behavior on T and c, the area of the droplets, and the similarity of their birefringence to that of the C_U phase in complementary solutions indicate that the duplexes are essentially insoluble in the isotropic and that the single-stranded DNA is essentially insoluble in the LC, as expected from theory (*35*).

This LC ordering thus requires the end-to-end stacking of the duplex sDNA into semirigid linear aggregates, which in turn means that within the LC drops the terminal groups on neighboring oligomers are close to each other and thus that their effective concentration is much higher than in the surrounding isotropic (*16*). This observation has potential implications for the prebiotic chemical generation of complementarily H-bonded molecular assemblies. In the presence of appropriate ligation chemistry, inorganic catalysts, for example (*36*), this concentration enhancement should strongly pro-

Fig. 3. (**A**) Nano-length B-DNA duplexes can be idealized as hydrophilic cylinders with hydrophobic ends capable of end-to-end adhesion and stacking into units sufficiently anisotropic to orientationally and positionally order into LC phases. The N phase is formed at lower concentration and the C_U phase at higher concentration. (**B**) Upon cooling a mixture of complementary (yellow/green) and noncomplementary (yellow/orange) single-stranded sDNAs, the complementary oligomers base pair to form duplexes, which then assemble as in (A) and phase-separate into LC domains. One way to achieve this is shown in (**C**), a 1:10 [Y (cyan): Z (magenta)] mixture of mutually complementary, but not self complementary, 12-nucleotide oligomers. Duplexes form upon cooling below their denaturation temperature T_m, and the LC phase appears below T_{LC} through a first-order phase transition, in this case a C_U phase. With one of the oligomer species in excess, in this case Z, the transition to the LC phase is marked by the appearance of isolated LC (C_U) domains that sequester all of the other complementary oligomer, in this case Y, into LC droplets. (C) shows a resulting DTLM image of LC domains. In the 1:10 case, the LC birefringence (comparable to that of the C_U phase in a 1:1 mixture) and the ~7% area occupied by LC domains is consistent with an essentially complete condensation of Y oligomers into the LC phase.
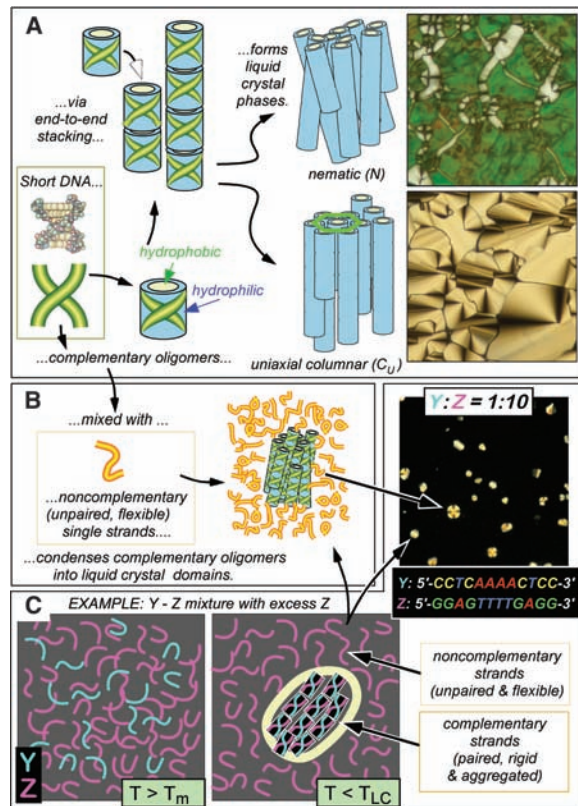
mote ligation in the LC phase relative to that in the isotropic. Additionally, every ligation in the LC phase produces an extended complementary oligomer. In this case, the formation of the LC phase by the complementary duplexes has the autocatalytic effect of establishing conditions that would strongly promote their own growth into longer complementary chains relative to the non–LC-forming oligomers. The fact that the liquid crystal ordering is found to depend sensitively on complementarity introduces selectivity into this process and means that the overall structure of the complementary assemblies generated will actually be templated by the liquid crystal geometry. This appears to have been the case for the linear rodlike structure of base-paired polynucleotides.

References and Notes

1. R. E. Franklin, R. G. Gosling, *Nature* **171**, 740 (1953).
2. J. E. Lydon, *Liq. Cryst. Today* **12**, 1 (2003).
3. M. H. F. Wilkins, A. R. Stokes, H. R. Wilson, *Nature* **171**, 738 (1953).
4. V. Luzzati, V. A. Nicolaieff, *J. Mol. Biol.* **1**, 127 (1959).
5. C. Robinson, *Tetrahedron* **13**, 219 (1961).
6. F. Livolant, A. M. Levelut, J. Doucet, J. P. Benoit, *Nature* **339**, 724 (1989).
7. R. L. Rill, T. E. Strzelecka, M. W. Davidson, D. H. van Winkle, *Physica A* **176**, 87 (1991).
8. K. Merchant, R. L. Rill, *Biophys. J.* **73**, 3154 (1997).
9. F. Livolant, F. A. Leforestier, *Prog. Polym. Sci.* **21**, 1115 (1996).
10. R. Podgornik, H. H. Strey, V. A. Parsegian, *Curr. Opin. Colloid Interface Sci.* **3**, 534 (1998).
11. R. Brandes, D. R. Kearns, *Biochemistry* **25**, 5890 (1986).
12. T. M. Alam, G. Drobny, *J. Chem. Phys.* **92**, 6840 (1990).
13. P. J. Hagerman, *Annu. Rev. Biophys. Biophys. Chem.* **17**, 265 (1988).
14. L. Onsager, *Ann. N.Y. Acad. Sci.* **51**, 627 (1949).
15. P. Bolhuis, D. Frenkel, *J. Chem. Phys.* **106**, 666 (1997).
16. Materials and methods are available as supporting material on *Science* Online.
17. M. P. Taylor, J. Herzfeld, *Langmuir* **6**, 911 (1990).
18. X. Lu, J. T. Kindt, *J. Chem. Phys.* **120**, 10328 (2004).
19. P. Van der Schoot, M. E. Cates, *Langmuir* **10**, 670 (1994).
20. R. Hentschke, J. Herzfeld, *Phys. Rev. A* **44**, 1148 (1991).
21. J. V. Selinger, R. F. Bruinsma, *Phys. Rev. A* **43**, 2922 (1991).
22. V. R. Horowitz, L. A. Janowitz, A. L. Modic, P. A. Heiney, P. J. Collings, *Phys. Rev. E Stat. Nonlin. Soft Matter Phys.* **72**, 041710 (2005).
23. R. Wing *et al.*, *Nature* **287**, 755 (1980).
24. M. R. Redinbo, L. Stewart, P. Kuhn, J. J. Champoux, W. G. J. Hol, *Science* **279**, 1504 (1998).
25. C. A. Davey, D. F. Sargent, K. Luger, A. W. Maeder, T. J. Richmond, *J. Mol. Biol.* **319**, 1097 (2002).
26. J. E. Lydon, *Curr. Opin. Colloid Interface Sci.* **8**, 480 (2004).
27. J. T. Davis, *Angw. Chem. Int. Ed.* **43**, 668 (2004).
28. M. A. Bates, D. Frenkel, *J. Chem. Phys.* **109**, 6193 (1998).
29. A. M. Bohle, R. Holyst, T. Vilgis, *Phys. Rev. Lett.* **76**, 1396 (1996).
30. H. Durchschlag, in *Thermodynamic Data for Biochemistry and Biotechnology*, H. J. Hinz, Ed. (Springer-Verlag, New York, 1986), chap. 3.
31. M. Mandelkern, J. G. Elias, D. Eden, D. M. Crothers, *J. Mol. Biol.* **152**, 153 (1981).
32. P. L. C. Teixeira, J. M. Tavares, M. M. Telo da Gama, *J. Phys. Condens. Matter* **12**, R411 (2000).
33. B. Tinland, A. Pluen, J. Strum, G. Weill, *Macromolecules* **30**, 5763 (1997).
34. S. Asakura, F. Oosawa, *J. Chem. Phys.* **22**, 1255 (1954).
35. P. J. Flory, *Macromolecules* **11**, 1138 (1978).
36. J. P. Ferris, G. Ertem, *Science* **257**, 1387 (1992).
37. T.B., N.A.C., and M.N. conceived and initiated the study. M.N. and G.Z. designed and directed the experiments. M.N. fabricated the gradient cells and performed optical studies on them. G.Z. performed the interferometry to determine DNA concentration. G.Z. fabricated and performed optical studies on the complementary/noncomplementary mixture cells. M.N., G.Z., R.P., B.C., C.J., and J.C. performed the x-ray experiments. This work was supported by a Ministero dell'Università e della Ricerca grant COFIN-2004024508 (T.B. and G.Z), NSF grant DMR 0606528 (N.A.C. and M.N.), NSF Materials Research Science and Engineering Centers grant DMR 0213819 (N.A.C.), and DOE Nanoscale Science, Engineering, and Technology Grant 04SCPE389 (R.P. and B.D.C.). Use of the Advanced Photon Source was supported by the U.S. Department of Energy under contract DE-AC02-06CH11357.

A High-Frequency Secondary Event During the 2004 Parkfield Earthquake

Bettina P. Allmann* and Peter M. Shearer

By using seismic records of the 2004 magnitude 6.0 Parkfield earthquake, we identified a burst of high-frequency seismic radiation that occurred about 13 kilometers northwest of the hypocenter and 5 seconds after rupture initiation. We imaged this event in three dimensions by using a waveform back-projection method, as well as by timing distinct arrivals visible on many of the seismograms. The high-frequency event is located near the south edge of a large slip patch seen in most seismic and geodetic inversions, indicating that slip may have grown abruptly at this point. The time history obtained from full-waveform back projection suggests a rupture velocity of 2.5 kilometers per second. Energy estimates for the subevent, together with long-period slip inversions, indicate a lower average stress drop for the northern part of the Parkfield earthquake compared with that for the region near its hypocenter, which is in agreement with stress-drop estimates obtained from small-magnitude aftershocks.

The 2004 magnitude (M) 6.0 Parkfield earthquake on the San Andreas Fault (SAF) in central California was well recorded by a dense network of seismic and geodetic sensors installed in anticipation of this event. The wealth of available data permits studying the rupture process of a moderate-sized crustal earthquake in detail. Results to date show

that the earthquake ruptured about 20 km northward from the hypocenter over about 10 s. However, ground accelerations near the fault exhibit large variations, and the high-frequency (HF) waves radiated by the earthquake are not yet fully understood. We show that a large burst of HF energy occurred about 5 s into the earthquake, as seen both in full-waveform back projection of strong motion data and in the timing of a clear secondary arrival that is observed on many of the records.

We used acceleration data from the General Earth Observing System (GEOS) array, the California Geological Survey (CGS) array, and

the U.S. Geological Survey (USGS) Parkfield dense seismograph array (UPSAR). These overlapping arrays were installed in the Parkfield region over the past 2 decades in order to record an expected M 6.0 earthquake (1). The CGS array consists mostly of analog stations that are triggered on the shear wave (S) arrival. These data are available in digital form with a 200-Hz sample rate (2). Altogether, there are 73 strong motion records from these networks in a 20-km radius around the Parkfield rupture area.

These data have been used to characterize strong ground motions from the mainshock and to invert for time-dependent slip models. These inversions are generally performed at relatively long periods because of the difficulty in fitting the more variable and incoherent HF part of the records. A different approach for imaging the earthquake rupture is by means of a back projection of the seismic waveforms into the volume surrounding the rupture (3). This method was first applied to rupture imaging of the 2004 Sumatra-Andaman earthquake with the use of teleseismic P records (4). For Parkfield, we stacked S waves on the north component from 68 out of 73 local strong-motion records along the travel-time operator obtained by ray tracing from each image point to each receiver through a reference one-dimensional (1D) velocity model. We forced the onset of waveforms to focus at the known hypocenter location of the mainshock by applying a static correction for each S arrival before stacking. This corrects for time shifts

Cecil H. and Ida M. Green Institute of Geophysics and Planetary Physics, Scripps Institution of Oceanography, University of California San Diego, 9500 Gilman Drive, La Jolla, CA 92093–0225, USA.

*To whom correspondence should be addressed. E-mail: ballmann@ucsd.edu

Science

End-to-End Stacking and Liquid Crystal Condensation of 6– to 20–Base Pair DNA Duplexes

Michi Nakata, Giuliano Zanchetta, Brandon D. Chapman, Christopher D. Jones, Julie O. Cross, Ronald Pindak, Tommaso Bellini and Noel A. Clark

ARTICLE TOOLS	http://science.sciencemag.org/content/318/5854/1276
SUPPLEMENTARY MATERIALS	http://science.sciencemag.org/content/suppl/2007/11/20/318.5854.1276.DC1
REFERENCES	This article cites 34 articles, 2 of which you can access for free http://science.sciencemag.org/content/318/5854/1276#BIBL
PERMISSIONS	http://www.sciencemag.org/help/reprints-and-permissions

Use of this article is subject to the Terms of Service